Chapter 1

Robustness of oscillations in biological systems

Jongrae Kim and Declan G. Bates

The oscillations observed in biological systems display a rich variety of dynamics and are typically generated by sophisticated multivariable feedback control mechanisms whose underlying design principles are obscure. It is hardly surprising then, that the study of such systems using mathematical techniques, including methods from systems and control engineering, has a long and varied history [Rapp, 1975, Linkens, 1979, Kholodenko et al., 1997, Goldbeter, 1997]. Until relatively recently, however, most such analyses of oscillatory biological systems have concentrated on establishing conditions for nominal stability or performance properties of the oscillations, with perhaps some investigation of the effect of varying individual parameters using phase plane analysis. This is hardly surprising, as many of these studies were undertaken long before the issue of robustness had come to dominate mainstream control theory. Additionally, because oscillations in physical engineering systems are typically problems to be avoided, relatively few robust control theorists have been interested in developing analytical techniques to analyse their robustness. Recent recognition of the potential of robustness analysis methods to help in the development, refinement and (in)validation of mathematical models of biological systems has radically altered this situation, however, and intensive efforts are now underway to develop analytical techniques to quantify the robustness of models of oscillatory

biological systems. In this chapter, we describe a number of promising methods for the robustness analysis of such systems, and show how such analysis can shed new insight into the underlying design principles of the systems concerned. We apply the proposed methods to analyse the robustness of oscillations in the concentration of adenosine $3'$, $5'$-cyclic monophosphate (cAMP) which have been observed during the aggregation phase of starvation-induced development in *Dictyostelium discoideum*. We also highlight the important roles played by stochastic noise in ensuring the robustness of biological oscillations.

1.1 Robust cAMP oscillations in aggregating *Dictyostelium* cells

Dictyostelium discoideum are social amoebae which normally live in forest soil, where they feed on bacteria [Othmer & Schaap, 1998]. Under conditions of starvation, *Dictyostelium* cells begin a programme of development during which they aggregate and eventually form spores atop a stalk of vacuolated cells. At the beginning of this process the amoebae become chemotactically sensitive to cAMP and, by six to ten hours, almost all of them acquire competence to relay cAMP signals [Gingle & Robertson, 1976]. After eight hours, a few pacemaker cells start to emit cAMP periodically [Raman et al., 1976]. Surrounding cells move towards the cAMP source and relay the cAMP signal to more distant cells. Eventually, the entire population collects into mound shaped aggregates containing up to 10^5 cells [Coates & Harwood, 2001]. The processes involved in cAMP signalling in *Dictyostelium* are mediated by a family of cell surface cAMP receptors (cARs) that act on a specific heterotrimeric G protein to stimulate actin polymerisation, activation of adenylyl and guanylyl cyclases and a number of other responses [Parent & Devreotes, 1996]. Most of the components of these pathways have mammalian counterparts, and much effort has been devoted in recent years to the study of signal transduction mechanisms in these simple microorganisms, with the eventual aim of improving understanding of defects in these pathways which may lead to disease in humans [Williams et al., 2006].

[Laub & Loomis, 1998] proposed a network model of interacting proteins that can account for the spontaneous oscillations in adenlylate cyclase activity that are observed in homogeneous populations of *Dictyostelium* cells four hours after the initiation of development. Analyses of the numerical solutions of the

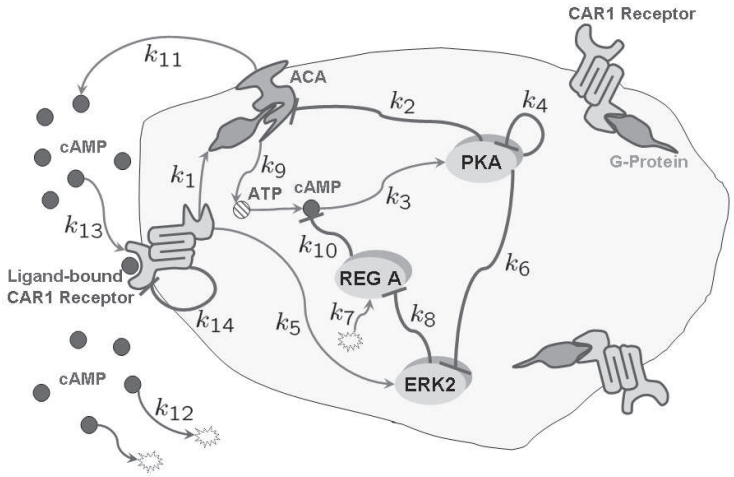

Figure 1.1: *Dictyostelium discoideum* cAMP oscillation network. The normal arrows indicate activation or self-degradation and the bar arrows indicate inhibition.

nonlinear differential equations making up the model suggest that it faithfully reproduces the observed periodic changes in adenosine 3′,5′-cyclic monophosphate (cAMP). In particular, periods, amplitudes and phase relations between oscillations in enzyme activities and internal and external cAMP concentrations were seen to agree well with experimental observations, [Laub & Loomis, 1998].

The Laub-Loomis model for the cAMP oscillations is given by a set of seven nonlinear coupled ordinary differential equations as follows:

$$\frac{dx_1}{dt} = k_1 x_7 - k_2 x_1 x_2, \tag{1.1a}$$

$$\frac{dx_2}{dt} = k_3 x_5 - k_4 x_2, \tag{1.1b}$$

$$\frac{dx_3}{dt} = k_5 x_7 - k_6 x_2 x_3, \tag{1.1c}$$

$$\frac{dx_4}{dt} = k_7 - k_8 x_3 x_4, \tag{1.1d}$$

$$\frac{dx_5}{dt} = k_9 x_1 - k_{10} x_4 x_5, \tag{1.1e}$$

$$\frac{dx_6}{dt} = k_{11} x_1 - k_{12} x_6, \tag{1.1f}$$

$$\frac{dx_7}{dt} = k_{13} x_6 - k_{14} x_7, \tag{1.1g}$$

Parameter	**Nominal Values**	**Parameter**	**Nominal Values**
k_1 [1/min]	2.0	k_8 [1/(μM min)]	1.3
k_2 [1/(μM min)]	0.9	k_9 [1/min]	0.3
k_3 [1/min]	2.5	k_{10} [1/(μM min)]	0.8
k_4 [1/min]	1.5	k_{11} [1/min]	0.7
k_5 [1/min]	0.6	k_{12} [1/min]	4.9
k_6 [1/(μM min)]	0.8	k_{13} [1/min]	23.0
k_7 [μM/min]	1.0	k_{14} [1/min]	4.5

Table 1.1: The kinetic constants : Nominal value

where t is time, x_1 is adenlylate cyclase (ACA), x_2 is the protein kinase A (PKA), x_3 is the MAP kinase (ERK2), x_4 is intracellular phosphodiesterase (REG A), x_5 is internal cAMP, x_6 is external cAMP, and x_7 is the high-affinity cell surface cAMP receptor CAR1. The nominal values for the kinetic constants, k_i, are given in Table 1.1. Note that all quantities are given as concentrations, i.e. Molar (mole/litre). The interaction network described by the model is shown in Fig. 1.1. After external cAMP binds to the cell surface receptor CAR1, CAR1 activates adenylyl cyclase ACA and the mitogen activated protein kinase ERK2. ACA stimulates the production of intracellular cAMP, which in turn, activates the protein kinase PKA. PKA inhibits ACA and ERK2, which form two negative feedback loops controlling the level of internal cAMP. PKA activity is decreased as the internal cAMP is hydrolyzed by REG A. The internal cAMP is secreted to the outside of the cell and diffuses between cells. Thus, when external cAMP binds to CAR1 this forms a positive feedback loop.

In the remainder of this chapter, three different approaches for the robustness analysis of uncertain systems are applied to the above network model. Here, robustness is defined as the ability of the biochemical network model to reproduce the experimentally observed oscillations in cAMP, ACA, etc. in the presence of realistic levels of variation in multiple kinetic parameters. The first method measures local stability robustness properties of the oscillations using the structured singular value μ, a tool developed in the field of robust control theory to measure the robustness of feedback control systems to multiple forms of uncertainty. The second method uses a global optimisation algorithm to search for the smallest variation in the nonlinear model parameters which drives the states

of the system to a non-oscillatory behaviour. Finally, a stochastic analysis is performed using Monte-Carlo simulation to highlight the significant effect that intracellular noise can have on the robustness of biomolecular networks.

1.2 Deterministic robustness analysis

1.2.1 Local robustness analysis

The structured singular value or μ-analysis method is a standard tool for the robustness analysis of linear systems in feedback control engineering [Balas et al., 2008]. To make it easier to understand the basic concepts and formulations of μ-analysis, consider the following simple ordinary differential equation:

$$\frac{dx(t)}{dt} = kx(t), \tag{1.2}$$

where $x(t)$ is the concentration of some molecular species which degrades with the rate k. Let the rate be given by $k = -2(1+\delta)$, where δ is the uncertainty in the estimate of the kinetic rate constant. The concentration of x converges to zero exponentially as t increases if k is strictly less than zero, since the solution to the differential equation is given by $x(t) = x_0 e^{-2(1+\delta)t}$, where x_0 is the initial concentration of x. The necessary and sufficient condition for $x(t)$ to converge to zero, i.e. for the system to be stable, is that the exponent is strictly less than zero. For this case, it is given by $\delta > -1$. Similarly, for the vector case,

$$\frac{d\mathbf{x}(t)}{dt} = K(\boldsymbol{\delta})\mathbf{x}(t) \tag{1.3}$$

where $\mathbf{x}(t)$ is an n-dimensional non-negative real vector, whose elements represent the concentration of different molecular species, and $K(\boldsymbol{\delta})$ is a kinetic rate matrix whose dimension is $n \times n$ and whose value is a function of the uncertain vector $\boldsymbol{\delta}$ whose dimension is p. Again, the solution is given by $\mathbf{x}(t) = \mathbf{x}_0 e^{-K(\boldsymbol{\delta})t}$. Note that for the vector case the exponential is the matrix exponential (See Chapter 1). Similar to the scalar case, the necessary and sufficient condition for $\mathbf{x}(t)$ to converge to zero as t increases is that all the real parts of the eigenvalues of $K(\boldsymbol{\delta})$ are strictly less than zero [Chapter 1]. However, it is well known that eigenvalues are often poor measures of robustness [Doyle & Stein, 1981]. That is, there are many cases where a tiny perturbation could make the trajectories diverge to infinity, i.e. become unstable, for a specific uncertainty, even when

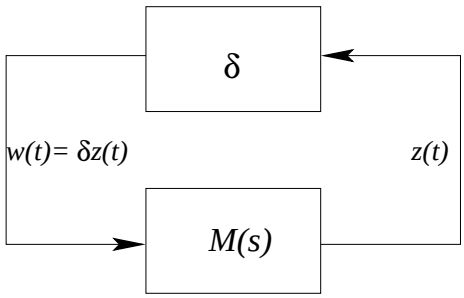

Figure 1.2: M-Δ structure for μ-analysis.

the eigenvalues are far away from the positive real region. In robust control theory, the following alternative approach is usually adopted to avoid this problem [Balas et al., 2008]. Consider the scalar example, Eq. (1.2), for k equal to $-2(1+\delta)$. It can be rewritten as follows by decoupling the known part and the uncertain part:

$$\frac{dx(t)}{dt} = -2x(t) + w(t) \tag{1.4a}$$

$$z(t) = -2x(t) \tag{1.4b}$$

where the uncertain part $w(t)$ is given by $\delta z(t)$. Hence, the above system considers the effect of the uncertain part, $w(t)$, as an input to the system and $w(t)$ is given by the product of the system output, $z(t)$, by the uncertain gain, δ. This decoupling is always possible when the uncertain parameter, δ, appears as a rational polynomial function form, and the resulting problem formulation is called a Linear Fractional Transformation (LFT) [Chapter 1]. Using the Laplace transform, Eq. (1.4) may be transformed to give the input, $w(t)$, and the output, $z(t)$, relation as follows:

$$Z(s) = M(s)W(s) \tag{1.5}$$

where s denotes the Laplace transform, $Z(s)$ and $W(s)$ are the Laplace transforms of $z(t)$ and $w(t)$, respectively, and

$$M(s) = -\frac{2}{s+2} \tag{1.6}$$

The LFT formulation is shown in Fig. 1.2 and it forms a self feedback loop. $M(s)$ can be considered as a system whose input is $w(t)$ and output is $z(t)$. As $M(s)$ is a linear system, the response is characterised completely by the

frequency response. That is, now we break the self feedback loop and introduce the sinusoidal input $w(t)$, whose frequency ranges from 0 to infinity. At each frequency, when $z(t)$ reaches a steady state oscillation, we instantly re-connect the feedback loop and observe how the internal signal changes. It may converge to zero or diverge to infinity as time increases. Mathematically, this can be done by substituting $W(s) = \delta Z(s)$ and $s = j\omega$ into Eq. (1.5). Then, we have that

$$[1 - M(j\omega)\delta]\, Z(j\omega) = 0 \tag{1.7}$$

where $j = \sqrt{-1}$ and ω is a non-negative real number. The physical meaning of this formulation can be appreciated by considering the frequency response of the system when it is excited with a sinusoidal signal whose frequency is ω. From Eq. (1.7), whenever $1 - M(j\omega)\delta \neq 0$, $Z(j\omega)$ is equal to zero. On the other hand, if $1 - M(j\omega)\delta = 0$, $Z(j\omega)$ is undefined. The above equality is the condition for some of the eigenvalues being located on the imaginary axis in the complex domain, i.e. the boundary of the stable/unstable regions. For the vector case, where the uncertain parameters are real numbers, δ will be a diagonal matrix, Δ, whose diagonal terms are given by the uncertain parameters and the singularity condition is given by the determinant as follows:

$$\det\left[I - M(j\omega)\Delta\right] = 0 \tag{1.8}$$

where I is the identity matrix whose dimension is the same as $M(j\omega)\Delta$. This is the condition for which the system becomes unstable. Hence, we want to try to calculate the Δ matrix which makes the determinant equal to zero. Of course, in general there will be an infinite number of Δ matrices which satisfy Eq. (1.8). Among these, we are interested in the uncertainty matrix whose magnitude is smallest, as this defines the smallest variation in the model parameters for which the system loses stability. Note that, although in theory this singularity condition must be checked at all frequencies $\omega \in [0, \infty)$, in practice it is usually sufficient to check for a finite number of grid points over the frequency range.

The structured singular value, $\mu(\omega)$, is thus defined as:

$$\frac{1}{\mu(\omega)} \triangleq \min_{\Delta} \{\bar{\sigma}(\Delta) | \det\left[I - M(j\omega)\Delta\right] = 0 \text{ for } \Delta \in B_\Delta\} \tag{1.9}$$

for $\omega \in [0, \infty)$, where $\bar{\sigma}(\cdot)$ denotes the maximum singular value, and B_Δ is a set defined by

$$B_\Delta = \{\Delta | \Delta = \text{diag}\left[\delta_1 I_1, \delta_2 I_2, \ldots, \delta_p I_p\right]\} \tag{1.10}$$

where diag[...] is a diagonal matrix, δ_i is the uncertain parameter and I_i is the identity matrix whose dimension could be one or more. The number of time an uncertain parameter is repeated, i.e. the dimension of I_i, depends on how the uncertain parameter appears in the equations describing the system, and constructing an LFT which has minimal dimensions for each I_i is sometimes not trivial. Calculating the value of μ exactly is usually prohibitively expensive from a computational point of view, and thus in practice the lower and the upper bounds on μ are generally computed. More details about μ-analysis can be found in [Balas et al., 2001] and [Skogestad & Postlethwaite, 2005].

We now describe the process of transforming the nonlinear oscillatory model, Eq. (1.1), into a form which can be used for μ-analysis. Let the original nonlinear differential equations for the model, Eq. (1.1), be written in compact form as

$$\frac{d\mathbf{x}}{dt} = \mathbf{f}(\mathbf{x},\, \mathbf{k}) \tag{1.11}$$

where $\mathbf{x} = [\, x_1,\, x_2, \ldots,\, x_7\,]^T$, $\mathbf{k} = [\, k_1,\, k_2, \ldots,\, k_{14}\,]^T$, $\mathbf{f}(\cdot,\cdot)$ is given by Eq. (1.1), and the superscript T is the transpose of a vector or matrix. Each kinetic parameter including uncertainty is given by

$$k_i = \bar{k}_i\,(1 + \delta_i) \tag{1.12}$$

for $i = 1, 2, \ldots, 13, 14$. With the nominal values of the k_i, given in Table 1.1, i.e. all δ_i's equal to zero, the model exhibits stable limit cycle trajectories in all states. To obtain the limit cycle model, a harmonic balance method is used [Ma & Iglesias, 2002]: first, the solution following the limit cycle, i.e., the nominal trajectory $x_i^*(t)$, can be written as

$$x_i^*(t) = a_{0,i} + \sum_{n=1}^{\infty} a_{n,i} \cos\left(\frac{2\pi n t}{\tau} + \phi_{n,i}\right) \tag{1.13}$$

for $i = 1,\, 2, \ldots,\, 7$, where τ is the period of the limit cycle. In practice, the upper bound of the summation is limited to a finite number.

Now, the nonlinear differential equation can be linearised about the nominal solution, $\mathbf{x}^*(t) = [\, x_1^*(t),\, x_2^*(t),\, \ldots,\, x_7^*(t)\,]^T$ and the model can thus be written as a linear periodically time-varying differential equation as follows:

$$\frac{d\mathbf{x}_{\text{pert}}}{dt} = A(t)\mathbf{x}_{\text{pert}} + B(t)\mathbf{w}_s(t) \tag{1.14a}$$

$$\mathbf{z}_s(t) = C(t)\mathbf{x}_{\text{pert}} + D(t)\mathbf{w}_s(t) \tag{1.14b}$$

where $A(t) = A(t+\tau)$, $B(t) = B(t+\tau)$, $C(t) = C(t+\tau)$, $D(t) = D(t+\tau)$ and each element of the $\mathbf{x}_{\text{pert}}$ is the perturbed state from x_i^* for $i = 1, 2, \ldots, 7$. In order to convert this model to a linear time-invariant system, the model is discretised, and a technique called "lifting", [Ma & Iglesias, 2002], is subsequently used to convert the resulting periodic state-space matrices to constant matrices. To do that, firstly, for a fixed time, t_k, which is an element of $[t, t+\tau)$, Eq. (1.14) is discretised as follows:

$$\mathbf{x}_{\text{pert}}(t_{k+1}) = \Phi(t_k)\mathbf{x}_{\text{pert}}(t_k) + \Gamma(t_k)\mathbf{w}_s(t_k) \tag{1.15a}$$

$$\mathbf{z}_s(t_k) = H(t_k)\mathbf{x}_{\text{pert}}(t_k) + J(t_k)\mathbf{w}_s(t_k) \tag{1.15b}$$

where

$$\Phi(t_k) = e^{F(t_k)h} \tag{1.16a}$$

$$\Gamma(t_k) = \left(\int_0^h e^{F(t_k)\eta} d\eta\right) B(t_k) \tag{1.16b}$$

$$H(t_k) = C(t_k)L^{-1}(t_k) \tag{1.16c}$$

$$J(t_k) = D(t_k) \tag{1.16d}$$

where $t_k = k\tau/n_{\text{dsc}}$ for $k = 0, 1, \ldots,$ and t_0 is set to zero without loss of generality. The approximation error can be reduced by increasing the number of discretisation points, n_{dsc}, although this also increases the dimension of the problem, and hence the resulting computational burden of the μ bound calculations, so in practice a sensible trade-off is required.

To demonstrate the lifting procedure, we first set k to zero. Then,

$$\mathbf{x}_{\text{pert}}(t_1) = \Phi(t_0)\mathbf{x}_{\text{pert}}(t_0) + \Gamma(t_0)\mathbf{w}_s(t_0) \tag{1.17}$$

and for $k = 1$,

$$\mathbf{x}_{\text{pert}}(t_2) = \Phi(t_1)\mathbf{x}_{\text{pert}}(t_1) + \Gamma(t_1)\mathbf{w}_s(t_1) \tag{1.18}$$

$$= \Phi(t_1)\left[\Phi(t_0)\mathbf{x}_{\text{pert}}(t_0) + \Gamma(t_0)\mathbf{w}_s(t_0)\right] + \Gamma(t_1)\mathbf{w_s}(t_1) \tag{1.19}$$

$$= \Phi(t_1)\Phi(t_0)\mathbf{x}_{\text{pert}}(t_0) + \begin{bmatrix}\Phi(t_1)\Gamma(t_0) & \Gamma(t_1)\end{bmatrix}\begin{bmatrix}\mathbf{w}_s(t_0)\\ \mathbf{w}_s(t_1)\end{bmatrix} \tag{1.20}$$

Subsequently, accumulating all $\mathbf{w}_s(t_k)$ from t_0 to $t_{n_{\text{dsc}}-1}$, and propagating the state $\mathbf{x}_{\text{pert}}(t_0)$ to $\mathbf{x}_{\text{pert}}(t_{n_{\text{dsc}}})$, a time-invariant discrete system is obtained. A

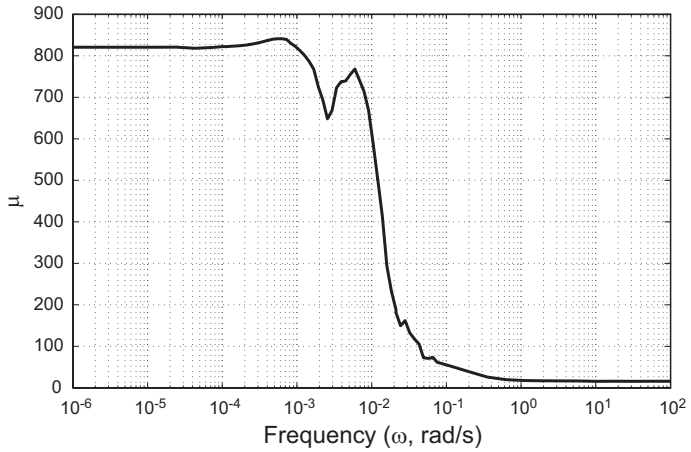

Figure 1.3: μ upper bound calculated using μ-toolbox at each ω [Balas et al., 2008].

similar procedure is also applied for $\mathbf{z}_s(k)$ and the corresponding matrices. Finally, using a zero-order hold or some other sampling method, the linear time-invariant discrete time system is transformed back to the continuous-time domain to give

$$\frac{d\mathbf{x}_{\text{pert}}(t)}{dt} = A\,\mathbf{x}_{\text{pert}}(t) + B\,\mathbf{w}(t) \tag{1.21a}$$

$$\mathbf{z}(t) = C\,\mathbf{x}(t) + D\,\mathbf{w}(t) \tag{1.21b}$$

where $\mathbf{x}_{\text{pert}}(t)$ is an arbitrary small perturbation away from $\mathbf{x}^*(t)$, $\mathbf{w}(t)$ is equal to $\Delta\,\mathbf{z}(t)$, and $\mathbf{w}(t)$ and $\mathbf{z}(t)$ are the accumulated vectors of $\mathbf{w}_s(t)$ and $\mathbf{z}_s(t)$ from the lifting procedure, respectively. More details of this transformation procedure can be found in [Kim et al., 2006b]. The system is now in the standard form for application of μ-analysis techniques, and $M(s)$ in Fig. 1.2 is given by

$$M(s) = C\,(sI - A)^{-1}\,B + D \tag{1.22}$$

The number of discretisation points, n_{dsc}, along the limit cycle is equal to 39, which is the minimum number of points so that the eigenvalues of A do not change by more than 0.001 for subsequent increases in n_{dsc}. Note that, as a result of the transformations described above the uncertainty matrix Δ is now made up of 39 repeated blocks of 13 real uncertain parameters. One of the

14 original uncertain parameters, k_7, does not appear as it is not multiplied by any x_i in Eq. (1.1). Hence, the robustness analysis results derived from this approach could slightly underestimate the effects of uncertainty on the system. Application of the standard algorithms for computing bounds on μ, [Balas et al., 2001], to the above system produced the results shown in Fig. 1.3. The inverse of the peak of the upper bound on μ provides a maximum allowable level of uncertainty for which stable oscillations in the original nonlinear system are guaranteed to persist. From the figure, however, this corresponds to a maximum allowable percentage variation in the parameters k_i of only $1/842 = 0.12\%$, indicating (possibly) very poor robustness indeed. Unfortunately, owing to the large number of repeated real parameters in the Δ matrix, the μ lower bound algorithms fail to converge and for the frequency range in the figure are all equal to zero. It is thus not possible to establish from this analysis whether the indicated lack of robustness is in fact true (μ is close to its upper bound), or not (μ is much smaller than the computed upper bound, i.e. the upper bound is conservative). In the next section we resolve this issue by means of a global analysis. Note however, that despite its various limitations, μ-analysis provides a rigorous and elegant framework for the robustness analysis of highly complex systems subject to multiple sources of uncertainty. Its main advantage over other methods is that it can provide deterministic guaranteed robustness bounds, which may easily be used to compare the relative robustness of different systems, or different models of the same system.

1.2.2 Global robustness analysis

An alternative approach to robustness analysis is to employ optimisation algorithms directly to search for particular combinations of parameters in the "uncertain parameter space" which maximise or minimise a particular cost function, whose value in some way reflects the level of robustness achieved by the model. Local optimisation methods, e.g. sequential quadratic programming (SQP), [MathWorks, 2006], that use gradient information are computationally efficient but can, of course, easily get locked into local optima in the case of multimodal search spaces. Global optimisation methods such as Genetic Algorithms (GAs) [Goldberg, 1989], on the other hand, use stochastic search and evolutionary principles to approach the true global optimum, albeit at the cost of significantly increased computation times. In the recent literature, several re-

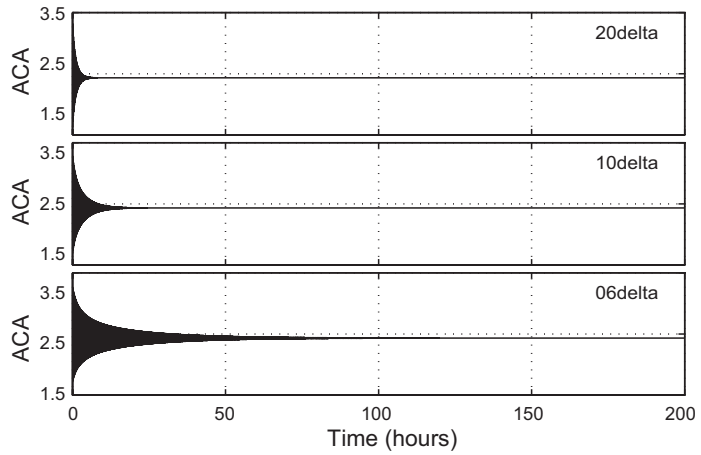

Figure 1.4: Effect of different levels of parameter variation on oscillatory behaviour. The global optimisation was performed on the interval from 10 hours to 20 hours and the longer simulations are shown to verify the results.

searchers have proposed combining the two approaches, [Davis, 1991, Yen et al., 1995]. [Lobo & Goldberg, 1996] provide some guidelines on designing hybrid GAs, along with experimental results and supporting mathematical analysis. In the present application, a probabilistic switching scheme based on that proposed in [Lobo & Goldberg, 1996] is used to dynamically switch between local (SQP) and global (GA) algorithms depending on which algorithm most effectively optimises the cost function at each iteration. Full details of the algorithm can be found in [Menon et al., 2006].

To apply the hybrid algorithm to test the robustness of the model's limit cycle the following cost function is defined to be minimized:

$$\min_{\boldsymbol{\delta}\in\Delta} J = \min_{\boldsymbol{\delta}\in\Delta} \int_{t_0}^{t_f} \dot{x}_1^2 \, dt \tag{1.23}$$

where

$$\Delta = \left\{ \boldsymbol{\delta} = [\delta_1, \delta_2, \ldots, \delta_{14}] \;\middle|\; \delta_i = \frac{p_\delta}{100} \times d_i \text{ for } i = 1, 2, \ldots, 14 \right\} \tag{1.24}$$

$d_i \in [-1,\, 1]$ for $i = 1,\, 2,\, \ldots, 14$, p_δ is the percentage level of uncertainty, which will be specified for each optimisation, and t_0 and t_f are chosen as 600 and 1200 minutes, respectively. Note that, unlike in the μ-analysis where δ_7 could

not be included, $\boldsymbol{\delta}$ now includes all δ_i from $i = 1$ to 14 . The reason for this choice of cost function is that the state derivative has to be zero whenever the states converge to a steady state and the limit cycle does not exist. The nonzero initial integration lower bound, $t_0 = 600$ minutes, is chosen to reduce the effect of initial transient responses on the cost function optimisation. Hence, the hybrid algorithm tries to find a $\boldsymbol{\delta}$ combination for the given boundary of p_δ, which minimises the cost function. After the minimum is found by the algorithm, it should be checked whether the state converges to an equilibrium point or not by integrating the nonlinear differential equations with the given values for the k_i for a number of different initial conditions. Depending on the existence of a limit cycle, p_δ is then increased or decreased until the minimum p_δ, denoted p_δ^*, is found to whatever desired accuracy. Results of the application of the hybrid optimisation algorithm are shown in Fig. 1.4, which shows ACA trajectories with the optimal combination of uncertainties in the set Δ for three different values of p_δ. For all three cases, the optimal $\boldsymbol{\delta}$ minimising the cost J occurs at the same boundary point, i.e.,

$$\boldsymbol{\delta}^* = \frac{p_\delta}{100}\,[-1,-1,1,1,-1,1,1,-1,1,1,-1,1,-1,1] \tag{1.25}$$

From the figure, it can be clearly seen that even for p_δ equal to 0.6 (corresponding to $\pm$ 0.6% variations in the parameters) the optimisation algorithm is able to find a parameter combination that destroys the limit cycle in the network model. As the allowable variation in the model parameters is increased, the rate of decay of the oscillations becomes even more rapid - for a $\pm 2\%$ variation the oscillations have completely ceased in less than 6 hours. Thus, our results confirm the poor robustness properties indicated in the previous μ-analysis, i.e. extremely small changes in the values of the model's parameters can destroy the required oscillatory behaviour.

1.3 Stochastic robustness analysis

The model for cAMP oscillations given in Eq. (1.1) in terms of ordinary differential equations corresponds to some original set of chemical reactions. Chemical reactions occur with certain probabilities proportional to the chances of collision of the molecules concerned. Let a molecule C be a complex, which is produced by the binding of two molecules A and B. If this reaction is observed

in a population of *Dictyostelium* cells, the reaction would be written as follows:

$$[\mathrm{A}] + [\mathrm{B}] \xrightarrow{k} [\mathrm{C}] \tag{1.26}$$

where $[\cdot]$ represents the concentration of each molecule. As each of the species (A, B and C) in the above is defined as a concentration of molecules, e.g. micro-Molar, the unit of k is given by $1/\mu\mathrm{M}/\mathrm{min}$, so that the following ordinary differential equation is properly defined:

$$\frac{d[C]}{dt} = k[A][B] \tag{1.27}$$

However, if one cell is observed instead of observing a population, then the chemical reaction is given by

$$\mathrm{A} + \mathrm{B} \xrightarrow{k/N_{\mathrm{av}}/V/10^{-6}} \mathrm{C} \tag{1.28}$$

where A, B and C are now in the units of numbers of each molecule. The rate k thus has to be transformed into $1/(\text{number of molecules})/\mathrm{min}$, for example. Hence,

$$\begin{aligned} k \left[\frac{1}{\mu\mathrm{M\ min}}\right] &= \frac{k}{10^{-6}} \left[\frac{\ell}{\mathrm{mole\ min}}\right] \\ \rightarrow \frac{k}{10^{-6}V} \left[\frac{1}{\mathrm{mole\ min}}\right] &= \frac{k}{10^{-6}N_{\mathrm{av}}V} \left[\frac{1}{\#\ \mathrm{min}}\right] \end{aligned} \tag{1.29}$$

where N_{av} is the Avogadro's number, 6.023×10^{23}, and V is the volume where the reaction occurs, e.g. the cell volume. Hence, the probability, P, that the reaction occurs for a unit time dt, is given by the product of the propensity function, a, and the unit time dt as follows:

$$P = a\ dt \tag{1.30}$$

where the propensity function, a, is given by

$$a = \frac{k}{10^{-6}N_{\mathrm{av}}V}AB \tag{1.31}$$

The length of the time interval at which the next reaction occurs follows the exponential distribution, and which reaction occurs at that instant depends on the propensity functions. An exact simulation algorithm, known as Gillespie's direct method, can be used to realise the given chemical master equation [Gillespie, 1977]. The details of the algorithm can be found in Chapter 2.

There could exist several variations on Eq. (1.28). Firstly, if A is relatively more abundant than B and C, then the number of A molecules is not significantly affected by the reaction. Then, A could be considered as a constant and the reaction could be modified as follows:

$$\mathrm{B} \xrightarrow{A \times k / N_{\mathrm{av}} / V / 10^{-6}} \mathrm{C} \tag{1.32}$$

That is, the C is directly produced from B and A is counted as a reaction rate. In addition, if B is also relatively abundant, then the reaction becomes

$$\varnothing \xrightarrow{A \times B \times k / N_{\mathrm{av}} / V / 10^{-6}} \mathrm{C} \tag{1.33}$$

Similar rules can be applied for the production side. Using these rules, we can reconstruct the corresponding chemical reactions to the Laub-Loomis model as follows:

$$\begin{aligned}
\mathrm{CAR1} &\xrightarrow{k_1} \mathrm{ACA} + \mathrm{CAR1} \\
\mathrm{ACA} + \mathrm{PKA} &\xrightarrow{k_2 / N_{av} / V / 10^{-6}} \mathrm{PKA} \\
\mathrm{cAMPi} &\xrightarrow{k_3} \mathrm{PKA} + \mathrm{cAMPi} \\
\mathrm{PKA} &\xrightarrow{k_4} \varnothing \\
\mathrm{CAR1} &\xrightarrow{k_5} \mathrm{ERK2} + \mathrm{CAR1} \\
\mathrm{PKA} + \mathrm{ERK2} &\xrightarrow{k_6 / N_{av} / V / 10^{-6}} \mathrm{PKA} \\
\varnothing &\xrightarrow{k_7 \times N_{av} \times V \times 10^{-6}} [\mathrm{RegA}] \\
\mathrm{ERK2} + \mathrm{RegA} &\xrightarrow{k_8 / N_{av} / V / 10^{-6}} \mathrm{ERK2} \\
\mathrm{ACA} &\xrightarrow{k_9} \mathrm{cAMPi} + \mathrm{ACA} \\
\mathrm{RegA} + \mathrm{cAMPi} &\xrightarrow{k_{10} / N_{av} / V / 10^{-6}} \mathrm{RegA} \\
\mathrm{ACA} &\xrightarrow{k_{11}} \mathrm{cAMPe} + \mathrm{ACA} \\
\mathrm{cAMPe} &\xrightarrow{k_{12}} \varnothing \\
\mathrm{cAMPe} &\xrightarrow{k_{13}} \mathrm{CAR1} + \mathrm{cAMPe} \\
\mathrm{CAR1} &\xrightarrow{k_{14}} \varnothing
\end{aligned} \tag{1.34}$$

where V equal to $3.672 \times 10^{-14} \ell$ is obtained by adjusting the volume so that the variable representing ligand-bound CAR1 is approximately matched to the

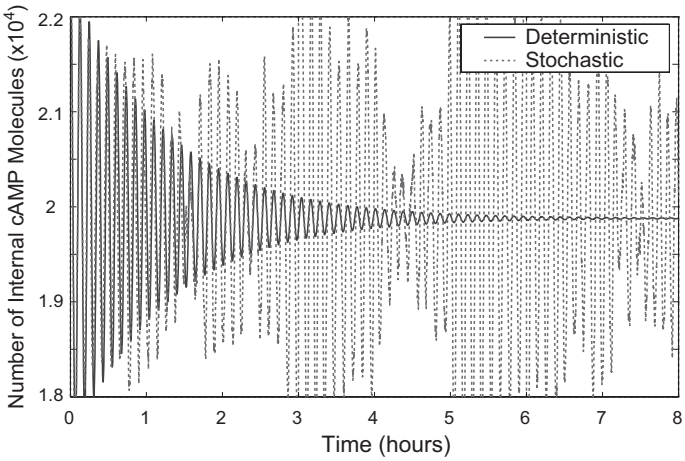

Figure 1.5: Internal cAMP oscillations with the worst case perturbation for the deterministic and the stochastic simulations.

known number of cell receptors on the surface of *Dictyostelium* cells [Laub & Loomis, 1998], i.e. about 40,000.

We can employ the above stochastic simulation approach to evaluate the effect of noise on the robustness of our model. As shown in Fig. 1.5, a 2% perturbation from the nominal values of the kinetic parameters in the original deterministic model is sufficient to destroy the stability of the oscillation and make the system converge to a steady state in about 6 hours [Kim et al., 2006a]. On the other hand, the figure shows that the stochastic model continues to exhibit a persistent oscillation for this perturbation to the nominal model parameters, when the stochastic simulation is performed using Gillespie's direct method [Gillespie, 1977]. Although these results mirror those of [Vilar et al., 2002] in revealing the qualitative differences in model dynamics which may result from consideration of noise, it is not yet clear whether the stochastic version of the model is actually more robust, as it could just be the case that a different worst-case parameter combination exists for this model. To clarify this issue, we proceed as follows. The kinetic parameters, the cell volume and the initial

conditions are all simultaneously perturbed according to:

$$k_i = \bar{k}_i \left(1 + \frac{p_\delta}{100}\ \delta_i\right) \tag{1.35a}$$

$$V = \bar{V} \left(1 + \frac{p_\delta}{100}\ \delta_v\right) \tag{1.35b}$$

$$x_i(0) = \bar{x}_i(0) \left(1 + \frac{p_\delta}{100}\ \delta_{x_i}\right) \tag{1.35c}$$

for $i = 1, 2, \ldots, 13, 14$, where the kinetic parameters are perturbed in the same way as the previous section, the nominal cell volume is equal to $3.672 \times 10^{-14}\ell$, the nominal initial conditions are as follows:

$$\bar{\mathbf{x}}(0) = \Big[7290, \quad 7100, \quad 2500, \quad 3000, \quad 4110, \quad 1100, \quad 5960\Big]^T \tag{1.36}$$

and δ_i, δ_v and δ_{x_i} are uniform random number in the range of $[-1, 1]$. As shown in Fig. 1.5, the number of molecules considered here is relatively large. The next reaction time of Gillespie's Direct method follows the exponential distribution whose exponent is the sum of all propensity functions. The *Dictyostelium* cAMP oscillation network has fourteen chemical reactions as given in Eq. (1.34). Hence, the value of the sum of all propensity functions is a large number and the time interval generated in the Gillespie's algorithm will be very small. As a result, the progress of the stochastic simulations will be very slow. To overcome this problem, a variation of the Gillespie's direct method is presented in [Gillespie, 2001], which is called the τ-leap algorithm. The accuracy of the algorithm is highly dependent on the local error tolerance chosen. By comparing the simulation results from the τ-leap and the Direct method for our example, the maximum allowed relative error was chosen to be 5×10^{-5}. The software package used for simulating the cAMP network using the τ-leap algorithm is called Dizzy, version 1.11.4, which is freely available [CompBio Group, Institute for Systems Biology, 2006].

Finally, 100 Monte-Carlo simulations are performed for random variations in the uncertain parameters for $p_\delta = 10\%$ and the time history of each internal cAMP variable is inspected. The time samples are obtained from 0 to 200 min with the sample time, 0.01 min. Then, the Fourier transform of the samples is taken using the FFT (fast Fourier Transform) algorithm in MATLAB [MathWorks, 2003]. To filter out non-oscillating cases, if the neighbourhood amplitudes around the peak amplitude are greater than 70%, then these are considered as non-oscillating cases. Exactly the same scenario was applied for the

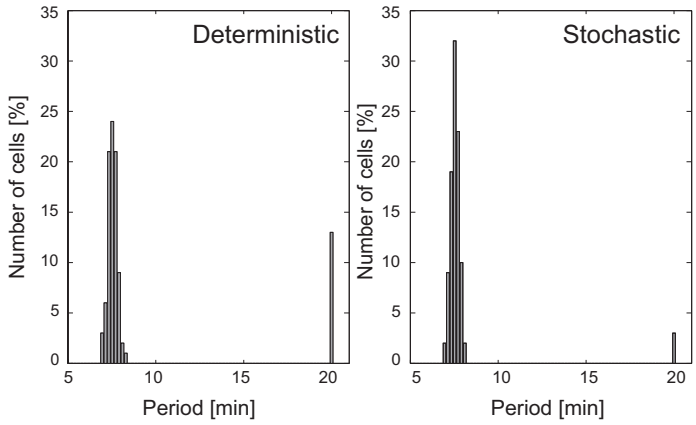

Figure 1.6: Period distributions for the deterministic and the stochastic simulations. The bars at 20 min represent the proportion of non-oscillating cases.

deterministic model and the final results are shown in Fig. 1.6. The bars at the 20 min mark on the x-axis represent the proportion of non-oscillating cases among the 100 simulations. For the deterministic model this is around 13% but for the stochastic model it is only 3%, thus the number of non-oscillating cases is significantly reduced by including the effects of stochasticity in the robustness analysis. The standard deviation of the period is also significantly reduced for the stochastic case, i.e. the changes in the period due to the effects of the uncertain parameters are smaller for the stochastic model than for the deterministic one. Similar improvements in the robustness of both the period and amplitude of the oscillations in the stochastic model were observed for a range of different uncertainty levels in the kinetic parameters, [Kim et al., 2007]. It is thus quite clear that stochastic noise in the *Dictyostelium* cAMP network represents an important source of robustness to variations between different cells and to changes in their environment.

1.4 Conclusions

In the recent Systems Biology literature, the concept of robustness has been proposed as a key indicator of validity for models of many types of biological systems. This chapter has shown how analysis tools from the field of control

engineering can be used to provide insight into the robustness of models of oscillatory biochemical networks. μ-analysis techniques provide allowable levels of parameter variations for which model robustness is guaranteed (something that optimisation-based search or statistical methods can never do). On the other hand, hybrid global/local optimisation methods can overcome the computational complexity of certain robustness analysis problems, and hence compute actual worst-case parameter combinations that can be used to check the theoretical robustness levels predicted by μ-analysis. Finally, statistical methods based on Monte-Carlo simulation allow a rigorous comparison of the robustness of deterministic and stochastic models of oscillatory biological systems. Such analysis reveals the crucial role played by intracellular noise in ensuring the robustness of the resulting oscillations. In this chapter, we have focused our analyses on individual *Dictyostelium* cells. As shown in [Kim et al., 2007], however, synchronisation effects between neighbouring cells can also have a significant impact on the robustness of the overall biological system. Stochastic simulations of large numbers of interacting cells require huge amounts of computing power, however, strongly motivating the development of analytical tools for evaluating the stability and robustness of stochastic systems — see [Scott et al., 2007] and [Kim et al., 2008] for some promising new results in this area.

Bibliography

Balas, G. J., Chiang, R., Packard, A. & Safonov, M. (2008). Robust Control Toolbox 3: User's Guide. The MathWorks, Inc., 3 Apple Hill Drive, Natick, MA 01760-2098, USA.

Balas, G. J., Doyle, J. C., Glover, K., Packard, A. & Smith, R. (2001). μ-Analysis and Synthesis Toolbox. The MathWorks, Inc., Natick, MA.

Coates, J. C. & Harwood, A. J. (2001). J. Cell Science 114, 4349–4358.

CompBio Group, Institute for Systems Biology (2006). http://magnet.systemsbiology.net/software/Dizzy.

Davis, L. (1991). Handbook of Genetic Algorithms. Van Nostrand Reinhold, New York.

Doyle, J. & Stein, G. (1981). IEEE Trans. Automatic Control 26, 4–16.

Gillespie, D. T. (1977). J. Physical Chemistry 81, 2340–2361.

Gillespie, D. T. (2001). J. Chemical Physics 115, 1716–1733.

Gingle, A. R. & Robertson, A. (1976). J. Cell Science 20, 21–27.

Goldberg, D. (1989). Genetic Algorithms for Search, Optimization, and Machine Learning. Addison Wesley Professional, Reading, MA.

Goldbeter, A. (1997). Biochemical Oscillations and Cellular Rhythms: The Molecular Bases of Periodic and Chaotic Behaviour. Cambridge University Press, Cambridge, UK.

Kholodenko, B. N., Demin, O. V. & Westerhoff, H. V. (1997). J. Physical Chemistry B 101, 2070–2081.

Kim, J., Bates, D., Postlethwaite, I., Ma, L. & Iglesias, P. (2006a). Systems Biology 153, 96–104.

Kim, J., Bates, D. G. & Postlethwaite, I. (2006b). Systems & Control Letters 55, 719–725.

Kim, J., Bates, D. G. & Postlethwaite, I. (2008). IEEE Trans. Automatic Control 53. In press.

Kim, J., Heslop-Harrison, P., Postlethwaite, I. & Bates, D. (2007). PLoS Computational Biology 3, e218.

Laub, M. & Loomis, W. (1998). Molecular Biology of the Cell 9, 3521–3532.

Linkens, D. A., ed. (1979). Biological Systems: Modelling and Control, vol. 11, of IEE Control Engineering series. Peregrinus, Stevenage, UK.

Lobo, F. & Goldberg, D. (1996). IlliGAL Report No. 96009, Tech. Report.

Ma, L. & Iglesias, P. (2002). BMC Bioinformatics 3, 38.

MathWorks (2003). Matlab User's Guide. The MathWorks, Inc., Natick, MA.

MathWorks (2006). Matlab Optimization Toolbox (*Version 3*). The MathWorks, Inc., Natick, MA, USA.

Menon, P. P., Kim, J., Bates, D. G. & Postlethwaite, I. (2006). IEEE Trans. Evolutionary Computation 10, 689–699.

Othmer, H. & Schaap, P. (1998). Comments on Theoretical Biology 5, 175–282.

Parent, C. & Devreotes, P. (1996). Annual Review Biochemistry 65, 411–440.

Raman, R. K., Hashimoto, Y., Cohen, M. H. & Robertson, A. (1976). J. Cell Science 21, 243–259.

Rapp, P. E. (1975). Mathematical Biosciences 25, 165–188.

Scott, M., Hwa, T. & Ingalls, B. (2007). Proc. National Academy Sciences USA 104, 7402–7407.

Skogestad, S. & Postlethwaite, I. (2005). Multivariable Feedback Control: Analysis and Design. 2nd edition, John Wiley & Sons Ltd., Chichester, UK.

Vilar, J., Kueh, H., Barkai, N. & Leibler, S. (2002). Proc. National Academy Sciences USA 99, 5988–5992.

Williams, R., Boeckeler, K., Graf, R., Muller-Taubenberger, A., Li, Z., Isberg, R., Wessels, D., Soll, D., Alexander, H. & Alexander, S. (2006). Trends in Molecular Medicine 12, 415–424.

Yen, J., Liao, J., Randolph, D. & Lee, B. (1995). In Proc. 11th IEEE Conference on Artificial Intelligence for Applications, IEEE Computer Society Press.